the reaction of **11** with acetyl chloride: D. J. Harris and V. Snieckus, unpublished results.
(26) An x-ray crystallographic analysis of **5** (trifluoroacetate salt) has been completed. All hydrogen atoms were located and refined. The overall geometry of the ligand in the cation is essentially that found for **2a–d** with the site of protonation being N_2: A. J. Carty, C. R. Jablonski, and N. J. Taylor, unpublished results.
(27) G. B. Gill, N. Gourlay, A. W. Johnson, and M. Mahendran, *Chem. Commun.* 631 (1969).
(28) B. F. G. Johnson, J. Lewis, P. McArdle, and G. L. P. Randall, *J. Chem. Soc., Dalton Trans.*, 456 (1972).
(29) M. Brookhart, E. R. Davis, and D. L. Harris, *J. Am. Chem. Soc.*, **94**, 7853 (1972).
(30) A. M. Brodie, B. F. G. Johnson, P. L. Josty, and J. Lewis, *J. Chem. Soc., Dalton Trans.*, 2031 (1972).
(31) G. E. Coates, M. L. H. Green, and K. Wade, "Organometallic Compounds," Vol. 2, M. L. H. Green, Ed., Methuen, London, 1968, p 211, and references therein; R. F. Heck, "Organotransition Metal Chemistry: A Mechanistic Approach", Academic Press, New York, N.Y., 1974, p 139.
(32) S. Braun and W. E. Watts, *J. Organomet. Chem.*, **84**, C33 (1975), and references therein.
(33) A. Ginsburg, V. N. Setkina, and D. N. Kursanov, *J. Organomet. Chem.*, **77**, C27 (1974).
(34) A. Ceccon and S. Sartori, *J. Organomet. Chem.*, **50**, 161 (1973); J. D. Holmes, D. A. K. Jones, and R. Pettit, *ibid.*, **4**, 324 (1965).
(35) R. E. Davis, H. D. Simpson, N. Grice, and R. Pettit, *J. Am. Chem. Soc.*, **93**, 6688 (1971).
(36) N. A. Clinton and C. P. Lillya, *J. Am. Chem. Soc.*, **92**, 3065 (1970).
(37) T. S. Sorensen and C. R. Jablonski, *J. Organomet. Chem.*, **25**, C62 (1970).
(38) D. F. Shriver, "The Manipulation of Air Sensitive Compounds", McGraw-Hill, New York, N.Y., 1969.

Contribution from the School of Chemical Sciences, University of Illinois, Urbana, Illinois 61801

The Ferric Tris(dithiocarbamate) Spin Equilibrium Revisited. Variable-Temperature (4.2–296 K) Magnetic Susceptibility, (30–300 K) Infrared, and (4.2–85 K) Electron Paramagnetic Resonance Data

GRETCHEN R. HALL[1] and DAVID N. HENDRICKSON*[2]

Received May 7, 1975 AIC50314P

Variable-temperature magnetic susceptibility (4.2–296 K), infrared (30–300 K), and electron paramagnetic resonance (4.2–85 K) data are reported for one high-spin and nine $^6A_1$–$^2T_2$ spin-equilibrium ferric dithiocarbamates and for two low-spin ruthenium dithiocarbamates. The susceptibility data for the spin-equilibrium systems are least-squares fit by diagonalizing the $^6A_1$ and $^2T_2$ matrices including spin–orbit, zero-field, and Zeeman interactions as a function of magnetic field. As has been indicated previously, it is shown that a good fit of the susceptibility data requires an additional parameter that multiplies at high temperatures the contribution of the $^6A_1$ state beyond that expected. In the past this parameter has been taken as the vibrational partition ratio between the $^6A_1$ and $^2T_2$ states or as a temperature-dependent energy difference between the same two states. Variable-temperature ir data for the spin-equilibrium ferric complexes generally show a $^6A_1$ iron–sulfur band system at $\sim$360 cm^{-1} which loses intensity to a multiplet of $^2T_2$ iron–sulfur bands in the range of $\sim$300–350 cm^{-1}. These ir observations tend to indicate that the vibrational partition factor derived from the susceptibility fitting is *not* correct. Close inspection of the ir data also shows that the energy difference between $^6A_1$ and $^2T_2$ barycenters is also probably *not* temperature dependent. It is suggested that both the $^2T_2$ and the $^6A_1$ ferric states are very vibronic and that this could explain the observed shifts. Infrared data are also reported for certain manganese(III), cobalt(III), and chromium(III) tris(dithiocarbamates). EPR data for the spin-equilibrium ferric systems are seen to serve two purposes. On the one hand, the presence of distinct high-spin and low-spin signals set an upper limit on the high- to low-spin flipping rate of $\sim 10^{10}$ sec^{-1}. Second, at temperatures approaching 4.2 K, signals are seen for the lowest Kramers doublet from the $^2T_2$ state and the magnitudes of $g_\parallel$ and $g_\perp$ again point to a vibronic system.

Introduction

As early as 1931 Cambi and coworkers[3] prepared iron(III) *N,N*-dialkyldithiocarbamates, the first compounds reported to exhibit a spin equilibrium. Since this initial work, the many reviews[4–8] are testimony to the considerable work on such spin-equilibria systems. The ferric tris(dithiocarbamates) [Fe(dtc)$_3$] are one of the most thoroughly studied of these. A considerable number of physical techniques (generally only to liquid nitrogen temperatures) have been employed.[4] From the many studies various interesting facts have surfaced. For instance, in a series of 20 Fe(dtc)$_3$ compounds with a variety of nitrogen substituents, all but four compounds have effective magnetic moments in solution (chloroform and benzene) which are similar to those that they have in the solid state.[9] Deviations of approximately $\pm$1.0 BM between the solid- and solution-state values are seen for the other four Fe(dtc)$_3$ species. With regard to such specific interactions, it is important to note that an x-ray crystal structure has been reported[10] for the dichloromethane solvate of tris(4-morpholinecarbodithioato-*S,S'*)iron(III). Also another very recent paper[11] has discussed the effects of environment, solution vs. solid, on the $^5T_{2g}$–$^1A_{1g}$ equilibrium for a series of Fe(II) complexes with hexadentate ligands.

Nevertheless, even with all of the work on the Fe(dtc)$_3$ systems there still remain some interesting and important questions—questions that apply to many spin-equilibria systems. It has been reported[12] that a theoretical fitting of magnetic susceptibility data down to 90 K for a series of intermediate-spin Fe(dtc)$_3$ complexes required a vibrational partition parameter to account for differences in FeS_6 vibrational frequencies of the $^6A_{1g}$ and $^2T_{2g}$ states. As an aside, it is to be noted that a mathematically equivalent approach is found in assuming that the energy separation between the barycenters of the $^6A_{1g}$ and $^2T_{2g}$ states is temperature dependent. This later approach has been used for $^5T_{2g}$–$^1A_{1g}$ Fe(II) systems where certain complexes show "abrupt" transitions in their μ_{eff} vs. temperature curves.[13] A very recent paper by Sorai and Seki[14] has presented heat capacity data for Fe(phen)$_2X_2$, X^- = NCS^- and $NCSe^-$, to show that the coupling between the electronic state and the phonon system plays a prominent role in the cooperative (abrupt) spin transitions observed for these compounds. In our work we have collected magnetic susceptibility data from 296 to 4.2 K for an extended series of Fe(dtc)$_3$ complexes and we have collected variable-temperature infrared data. These two types of data will be analyzed to investigate the need and validity of in-

corporating such a vibrational partition function into the susceptibility expression.

The second question of interest in our work relates to the rate of "spin flipping" (i.e., interconversions of a molecule from a low- to a high-spin state, or vice versa) for the various $Fe(dtc)_3$ complexes. In a broad sense our interest here grows out of the possibility that certain ferric cytochromes exist as $^6A_{1g}$–$^2T_{2g}$ spin-equilibria systems and that the spin-state conversion is coupled to electron transport.[15] For a few spin-equilibria systems the spin-flipping rate has been measured directly with the laser *T*-jump technique.[16] The spin-flipping rate for $Fe(dtc)_3$ species in solution has been indicated to be greater than 10^5 sec^{-1} by NMR studies.[4] The observation of an averaged ^{57}Fe Mössbauer signal for the "intermediate-spin" $Fe(dtc)_3$ species and an analysis of the temperature dependence of the quadrupole splitting led Rasmussen and Merrithew[17] to suggest that the ferric dithiocarbamates may be a "mixed-spin" system as discussed for iron(III) hemes initially by Harris[18] and, more recently, by Maltempo.[19] A mixed-spin species would exhibit a very rapid spin-state conversion. If average ^{57}Fe Mössbauer signals are seen for the $Fe(dtc)_3$ species, then the spin-flipping rate in the solid is greater than 10^7 sec^{-1}. It is relevant to mention that recently four tris(monothio-β-diketonato)iron(III) compounds, which also show the $^6A_{1g}$–$^2T_{2g}$ spin equilibrium, have been reported to give ^{57}Fe Mössbauer spectra simultaneously showing signals for both the low- and high-spin species.[20] Our approach in this work is to employ a battery of physical techniques (NMR, ^{57}Fe Mössbauer, EPR, and ir), each with its intrinsic time scale, to bracket the spin-state conversion rate for the $Fe(dtc)_3$ species.

Experimental Section

Analytically pure (see data in Table I[21]; School of Chemical Sciences' microanalytical laboratory) samples of $M(dtc)_3$ were prepared as reported in the literature: Fe(III),[9] Co(III),[22] Ru(III),[23] Cr(III),[24] and Mn(III).[25] Recrystallizations were carried out using chloroform; infrared, analytical, and melting point data were used to check for the presence of solvent in the crystals.

As described in a previous paper,[26] variable-temperature (4.2–296 K) magnetic susceptibility measurements were made with a PAR Model 150A magnetometer operated at 12.3 kG and with a $CuSO_4 \cdot 5H_2O$ standard. EPR spectra were recorded at both X- and Q-band frequencies. In the former case, a Varian E-9 spectrometer was used in conjunction with an Air Products Heli-tran liquid helium cooling system to maintain the sample temperature in the range 12–77 K. Q-Band work was performed with a Varian V-4561 microwave bridge and a 6-in. magnet equipped with tapered pole pieces to extend the highest field to 15.5 kG. A liquid helium (4.2 K) direct-immersion quartz Dewar was used. The $Fe(dtc)_3$ EPR samples were run as pure powdered solids, as 1% doped solids, and as chloroform glasses. The 1% $Fe(dtc)_3$ doped samples were prepared with $Co(dtc)_3$ substrates, which were made relatively Cu free by boiling a $CoCl_2 \cdot 6H_2O$ aqueous solution for 5 min with excess thioacetamide in advance of the precipitation of $Co(dtc)_3$. These Cu-free $Co(dtc)_3$ samples showed no EPR signal for a copper impurity. The chloroform glasses of $Fe(dtc)_3$ decompose slowly on standing; therefore, they were prepared and sealed under vacuum in a tube immediately before use.

Infrared spectra were run on CsI pellets and Nujol mulls using both Beckman IR-11 and Perkin-Elmer 457 spectrophotometers. Peak positions were calibrated with water vapor absorptions and are reproducible to ±1 cm^{-1}. Control of ir sample temperatures was effected with a Spectrim cryocooling module (Cryogenic Technology, Inc.), equipped with polyethylene windows. A beam condenser was used with the IR-11. The temperature of the sample holder was monitored with an iron-doped gold thermocouple; temperatures from 300 K down to a low of 20 ± 2 K were possible. It is difficult to monitor accurately the temperature of the sample itself. An upper limit for the lowest sample temperature was estimated as 30 K for CsI pellets and slightly higher for Nujol mulls. These estimates were secured by attaching the thermocouple directly to the sample in various ways.

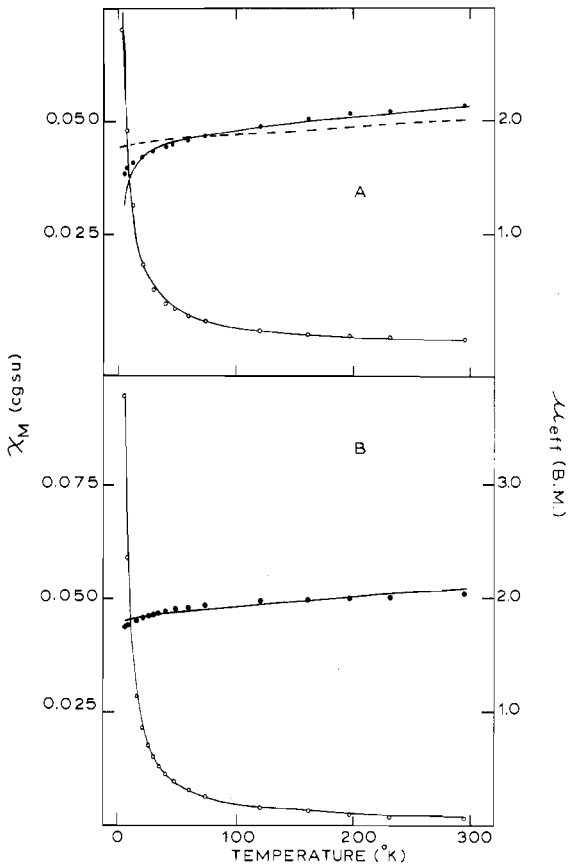

Figure 1. Temperature dependence of the magnetic susceptibility (open circles) and the magnetic moment (filled circles): A, $Ru(Et_2dtc)_3$; B, $Ru((n\text{-}Pr)_2dtc)_3$. The solid lines are generated from the theoretical best fit curves described in the text. The dashed line in curve A is for the rhombic $^2T_2$ magnetic moment curve generated from DeSimone's parameters.[34]

Results and Discussion

Magnetic Susceptibility. The metal ions in the $M(dtc)_3$ complexes are in trigonally compressed octahedral environments as shown by various x-ray structures: Fe(III) systems,[10,27,28] $Co(Et_2dtc)_3$,[29] and $Ru(Et_2dtc)_3$.[30]

Zero-field equations for the energy levels of a low-spin d^5 system including spin–orbit coupling[31] and trigonal distortion (gauged by *D*) are given in the literature.[32] A positive *D* value indicates a $^2E(d^2_{xy}d^3_{xz,yz})$ ground state with a $^2A(d^1_{xy}d^4_{xz,yz})$ excited state at a value of *D* higher in energy. The $Ru(dtc)_3$ complexes are low-spin d^5 systems and as such it was deemed desirable to determine the susceptibility characteristics of two ruthenium complexes. Figure 1 illustrates (see Table II[21] for data and fittings) the μ_{eff} vs. temperature data (points) for $Ru(Et_2dtc)_3$ and $Ru((n\text{-}Pr)_2dtc)_3$. In the latter case μ_{eff} varies smoothly and gradually from 2.04 BM at 295 K to 1.76 BM at 4.2 K which is quite characteristic of such a distorted t_{2g}^5 system. In the case of $Ru(Et_2dtc)_3$ the value of μ_{eff} varies from 2.13 BM at 295 K to 1.54 BM at 4.2 K. This latter value is, of course, below the spin-only value of 1.73 BM, possibly indicating a weak intermolecular exchange interaction. Such an interaction has been detected very recently with very low-temperature data on $Fe((pyrr)dtc)_3$.[33]

In collecting the μ_{eff} data for these two Ru(III) complexes, it was our major concern to see the susceptibility characteristics on our instrument of an analogous and totally low-spin d^5 system and to see if such data would give a fit in agreement with recently published[34] EPR data on $Ru(Et_2dtc)_3$. At the outset, it should be admitted that powder susceptibility data may yield inaccurate parameters when fitted without an-

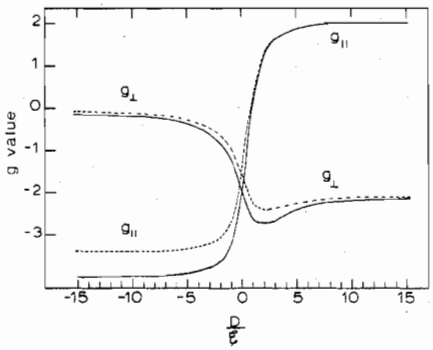

Figure 2. Variation of g values for $^2T_2$ states with the ratio of trigonal distortion to one-electron spin-orbit coupling constant. The solid lines are for the orbital reduction constant $k = 1.0$; the dotted lines are for $k = 0.7$.

isotropy data, as was demonstrated by Gregson and Mitra[35] for $Ru(acac)_3$.

The computer program STEPT[36] was used to fit the susceptibility data for $Ru((n\text{-}Pr)_2dtc)_3$. Exact matrix diagonalizations[37] were employed and by varying the initial values of D and k over a very extended range two different parameter fits (assuming $\xi = 1200$ cm^{-1}) are obtained: fit 1, $D = -970$ cm^{-1} and $k = 1.02$ (SE = 0.038); fit 2, $D = 930$ cm^{-1} and $k = 1.06$ (SE = 0.041). Thus, as anticipated, a fit with either positive or negative D can be obtained. In the case of the $Ru(Et_2dtc)_3$ data, however, a Weiss constant (Θ) was also used (i.e., replace T by $T - \Theta$) to give fit 1, $D = -410$ cm^{-1}, $k = 0.84$, and $\Theta = 1.7°$ (SE = 0.029); fit 2, $D = 920$ cm^{-1}, $k = 0.89$, and $\Theta = 4.5°$ (SE = 0.11). The parameter Θ merely handles the very low-temperature data and can be viewed as gauging intermolecular exchange interactions.[38] Solid lines are given in Figure 1 for the positive D fits. It is to be noted that for $Ru(Et_2dtc)_3$ only one of our two parameter fits is represented in the two fits obtained by DeSimone[34] from EPR data. He obtained and favored a fit where $D/\xi = 10.2$, that is, where there is a very large positive trigonal distortion parameter. The nature of the susceptibility fitting process and the probable reason for the minimization program STEPT not locating this particular DeSimone fit can be understood by recourse to Figure 2 where we have plotted $g_{\parallel}$ and $g_{\perp}$ vs. D/ξ (this is a much expanded version of the type of plot reported by Stanko et al).[39] In order to accommodate the degree of non-spin-only powder susceptibility and anisotropy seen in the EPR[35] ($g_{\parallel} = 1.99$ and $g_{\perp} = 2.13$) three regions of fitting are seen: $D/\lambda \simeq -1$, $D/\lambda \simeq +1$, and $D/\lambda \simeq -10$. In the first two cases the magnetic anisotropy is changing rapidly as a function of D/λ and STEPT secures minimizations, whereas, in the last case the anisotropy is changing slowly and STEPT apparently "overshoots" this minimum. Nevertheless, reference to Figure 1 shows (dashed line) that, if we take the parameters of DeSimone for $Ru(Et_2dtc)_3$ ($D/\xi = 10.2$ where $k = 0.7$ and $\xi = 1200$ cm^{-1}) in conjunction with a rather large TIP of 300×10^{-6} cgsu, moderate agreement with our susceptibility data is obtained. DeSimone did not study the $Ru((n\text{-}Pr)_2dtc)_3$ compound. The EPR data point to the preferred solution for the $Ru(dtc)_3$ systems, a solution wherein there is a large positive zero-field distortion.

Before the "intermediate-spin" $Fe(dtc)_3$ systems are considered, we present in Figure 3 and Table III[22] the susceptibility data obtained on our apparatus for the totally high-spin d^5 system $Fe((pyrr)dtc)_3$. Our data are in substantial agreement with those reported (295.5–2.26 K) by Figgis and Toogood,[40] who were not able to account totally for their data in terms of zero-field splitting of the $^6A_{1g}$ state. The success of a more recent theoretical analysis[41] incorporating high-order magnetic field effects and fourth-order ligand field terms has to be weighed against the report[33] of weak intermolecular

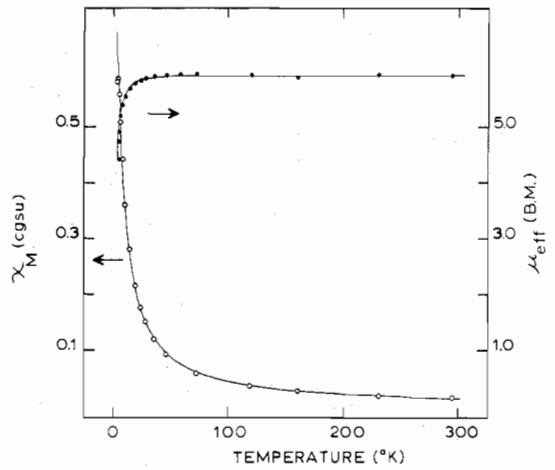

Figure 3. Temperature dependence of the magnetic susceptibility (open circles) and the magnetic moment (filled circles) for $Fe((pyrr)dtc)_3$. The solid lines are generated from the best fit theoretical curves discussed in the text.

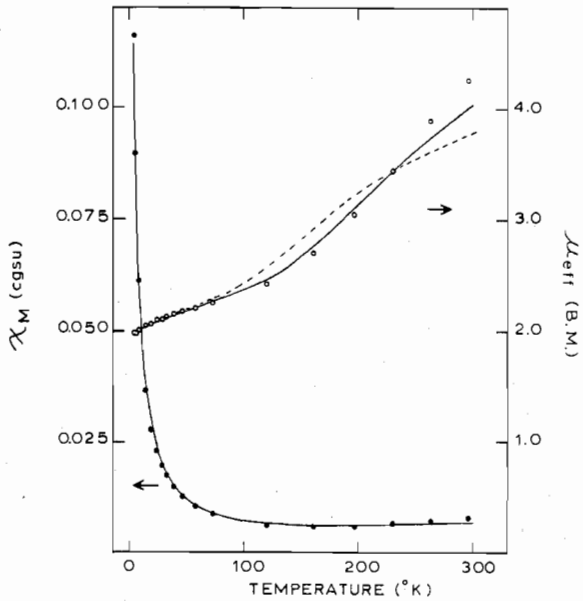

Figure 4. Temperature dependence of the magnetic susceptibility (filled circles) and the magnetic moment (open circles) for $Fe(Et_2dtc)_3$. The solid lines are generated from the best fit theoretical fit B of Table IX. The dotted line is theoretical curve A of Table IV.

exchange interactions (susceptibility maximum at ~2 K) for this same compound. The equations of Marathe and Mitra were used (6×6 matrix diagonalized as function of magnetic field at each temperature) with STEPT to fit our data. As indicated in Figure 3 and Table III,[22] a good fit (SE = 0.057) is obtained where the spin-Hamiltonian parameter B_4^0 is −0.39 cm^{-1} and with the constraints as established[41] we have $B_2^0 = -0.06$ and $B_4^3 = \pm 1.4$ cm^{-1}. In short, our data are in agreement with the previous report and can be fit with the equations for a $^6A_{1g}$ state. Accurate parameterization of the data very near 4.2 K is not important in our present study.

Variable-temperature magnetic susceptibility data down to 4.2 K have been collected for nine "intermediate-spin" $Fe(dtc)_3$ compounds. Some typical data are illustrated in Figures 4, 5,[21] 6, and 7;[21] the complete data sets for all nine compounds and theoretical fits are given in Tables IV–XII.[21] Before we describe our fits, previous susceptibility work on these systems is summarized. Ewald et al.[12] measured the susceptibilities of 18 ferric dithiocarbamates from room temperature to ~90 K and fit their data with the parameters g, C, and E. Here

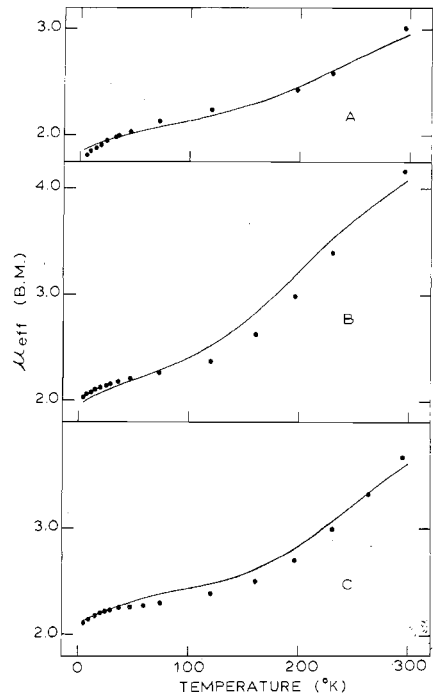

Figure 6. Temperature dependence of the magnetic moment: A, $Fe((i\text{-}Bu)_2dtc)_3$; B, $Fe((n\text{-pentyl})_2dtc)_3$; C, $Fe((n\text{-Hx})_2dtc)_3$. The solid lines are generated from the theoretical best fit B in Table VII, fit B in Table IX, and fit F in Table XII, respectively.

g is the g value for the $^2T_{2g}$ state and E is the energy separation between the zero-point levels of the $^2T_{2g}$ and $^6A_{1g}$ states. A spin–orbital interaction of $\lambda = -370$ cm^{-1} was assumed. The effects of trigonal distortion were, in part, accounted for with the parameter C; however, the main function of C was to account for the ratio of vibrational partition coefficients for the $^6A_{1g}$ and $^2T_{2g}$ levels. In other words, x-ray work[28] has shown that there is a difference of about 0.1 Å in Fe–S bond lengths for high-spin vs. low-spin ferric dithiocarbamates, and as such, the frequencies of the various Fe–S vibrational modes could be different for the two spin states. Ewald et al. were able satisfactorily to fit their data with the parameters g, E, and C. However, König and Kremer[13] attacked their treatment of the parameter C as having little physical meaning.

A second more refined treatment of the Ewald et al. data was carried out by Golding and de Lisle.[42] They included configuration interaction with excited electronic states, spin–orbital interaction of the $^2T_{2g}$ with the $^4T_{1g}$ state (some 7000 cm^{-1} above the ground state), and spin–orbital interaction of the $^6A_{1g}$ with the $^4T_{1g}$ state. In this treatment it was also necessary to include the vibrational partition coefficient ratio. Again, trigonal distortion of the $^2T_{2g}$ state was not explicitly treated; Figgis has shown that for data at higher temperatures (i.e., above ~90 K) μ_{eff} is not very sensitive to the trigonal distortion parameter D. In passing we should also note that Figgis and Toogood[40] reported the susceptibility of $Fe(Et_2dtc)_3$ from 4.2 to 100 K and fit their data with the equations for a $^2T_{2g}$ level including spin–orbital interaction and trigonal distortion D. The fit is good at the lower temperatures, but, as the temperature is increased, the experimental effective moments become increasingly greater than those predicted on the basis of a $^2T_2$ level only.

In the treatment of our 4.2–296 K susceptibility data for the nine "intermediate-spin" $Fe(dtc)_3$ species we have used the matrices for the $^2T_2$ state including spin–orbital and trigonal distortion interactions. The $Fe((pyrr)dtc)_3$ parameters (B_2^0, B_4^0, and B_4^3) were used as fixed numbers in the $^6A_1$ matrices. As was done above for the individual cases, the matrices for both the $^6A_1$ and $^2T_2$ states were diagonalized as a function of field at each parameter setting and the χ_{av} value was calculated as a Boltzmann-weighted average over the various levels. As parameters, then, we have λ ($=-k\xi$) and D (trigonal distortion) for the $^2T_2$ state, and the energy difference $\Delta E = E(^6A_1) - E(^2T_2)$, between the barycenters (zero-point levels) of the two states. Additional information is available.[43]

Several initial values of k (we assumed $\xi = 420$ cm^{-1} for the Fe(III) free ion), D, and ΔE were tried in fitting the $Fe(Et_2dtc)_3$ data as can be seen in Figure 4 and Table IV.[21] Without a vibrational partition factor, two relatively comparable but poor fits of the data are found with the parameters: fit A, $D = 366$ cm^{-1}, $\Delta E = 96$ cm^{-1}, and $k = 0.49$ (SE = 0.15); fit C, D = −961 cm^{-1}, $\Delta E = -67$ cm^{-1}, and $k = 0.56$ (SE = 0.20). In both cases (see Figure 4 for plotting of fit A as a dashed line) the fit is reasonable from 4.2 to ~80 K, but above 80 K the calculated and experimental effective moment curves have different shapes. In particular, at temperatures above ~230 K the calculated moments fall considerably below the experimental values. As per previous reports, a vibrational partition factor, Q(high spin)/Q(low spin) [Q(hs)/Q(ls)], was added to remedy this. The factor multiplies the $^6A_1$ contribution to the average susceptibility and its construction serves to give the $^6A_1$ state a proportionately greater contribution to the average susceptibility as the temperature is increased. The partition factor was taken as

$$\frac{Q(\text{hs})}{Q(\text{ls})} = \left[\frac{1 - e^{-\nu^s(^2T_2)/kT}}{1 - e^{-\nu^s(^6A_1)/kT}}\right]^6 \left[\frac{1 - e^{-\nu^b(^2T_2)/kT}}{1 - e^{-\nu^b(^6A_1)/kT}}\right]^9$$

Thus, there are six FeS_6 stretching frequencies (ν^s) and nine FeS_6 bending frequencies (ν^b). Ewald et al.[12] took $\nu^s(^2T_2) = 360$, $\nu^s(^6A_1) = 320$, $\nu^b(^2T_2) = 180$, and $\nu^b(^6A_1) = 160$ cm^{-1} and in this case at $T = 296$ K the value of Q(hs)/Q(ls) = 2.62. Figure 4 shows (solid lines) that an improved fitting of the high-temperature data is possible with such a partition factor and with $D = 378$ cm^{-1}, $\Delta E = 204$ cm^{-1}, and $k = 0.52$ the value of SE drops to 0.075 (fit B in Table IV).[21] Obviously, the fit can even be further improved by varying Q(hs)/Q(ls), and with the factor at 2.53, a least-squares analysis gives $D = 352$ cm^{-1}, $\Delta E = 250$ cm^{-1}, and $k = 0.50$ (SE = 0.038). In the upcoming infrared section it will be shown that the vibrational partition factor as presently formulated is probably not the cause of the unusual temperature dependence of the susceptibility of these $Fe(dtc)_3$ compounds. In passing we should note that the negative D fitting is improved with the inclusion of the vibration partition factor and gives the least-squares fit parameters $D = -925$ cm^{-1}, $\Delta E = 31$ cm^{-1}, $k = 0.55$, and SE = 0.072 (fit D in Table IV).[21] As we mentioned in the Introduction, the mathematically equivalent approach with a temperature-dependent ΔE gives fits to the data that are comparable to the partition factor model.

The addition of either TIP or interaction with the $^4T_1$ excited state to either of the above models would cause little change in the theoretical fitting of the high-temperature data. As has been noted,[12] the inclusion of a partition factor is generally necessary for intermediate-spin $Fe(dtc)_3$ species. The experimental susceptibility data for the other eight $Fe(dtc)_3$ compounds are given in Tables V–XII[21] and are illustrated in Figures 5,[21] 6, and 7.[21] The solid lines in Figures 5–7 are derived from theoretical fits including a vibrational partition factor (the same factor was used for all complexes and at 296 K the value was taken as 2.62 as indicated above). For three of the nine $Fe(dtc)_3$ compounds the low-temperature experimental moments are higher than the calculated values and as indicated in Figure 5[21] (tracing B) the fit can be improved by assuming a small (<5%) amount of high-spin ferric impurity. Table XIII gives the fitting parameters obtained for

Table XIII. Best Fit Parameters from Least-Squares Susceptibility Fittings

Compd	D, cm^{-1}	k	ΔE, cm^{-1}	E,[a] cm^{-1}	ΔE_{eff},[b] cm^{-1}
Fe((*n*-Bu)$_2$dtc)$_3$				−24	
141–296 K	384	0.08	−115		−56
4.2–137 K	384	0.47	−118		−6
Fe((*n*-Pr)dtc)$_3$				194	
B	383	1.10	−107		207
E	395	1.03	−78		216
F	−598	1.18	−157		217
Fe((*n*-pentyl)$_2$dtc)$_3$					
B	357	0.40	220		314
D	−795	0.36	113		257
Fe(Me$_2$dtc)$_3$				392	
A	373	0.80	63		
B	377	0.80	110		317
C	−619	0.78	−7		
D	−636	0.79	41		282
Fe(Et$_2$dtc)$_3$					
A	366	0.49	96		
B	378	0.52	204		279
C	−961	0.56	−67		
D	−925	0.55	31		356
Fe((allyl)$_2$dtc)$_3$				267	
B	378	0.71	205		385
E	267	0.60	372		523
F	−468	0.68	213		328
Fe((*n*-Hx)$_2$dtc)$_3$				594	
B	382	0.41	335		435
D	−709	0.15	237		
F	−801	0.58	197		417
Fe((*i*-Bu)$_2$dtc)$_3$				890	
B	387	0.95	276		538
D	−386	0.98	304		556
Fe((*i*-Pr)$_2$dtc)$_3$				1411	
B	386	0.43	563		669
D	−915	0.37	435		630

[a] Reference 12. [b] ΔE_{eff} is effective energy separation between the $^6A_1$ barycenter and the lowest Kramers doublet. This is determined from the expression $e^{-\Delta E_{eff}/kT} = e^{-E'/kT}$ where $E' = E(^6A_1) - E$(ground state) and $Q = 2.62$ (i.e., room-temperature value). [c] The different letters refer to the various theoretical fitting models given the tables of susceptibility data (see text).

the nine Fe(dtc)$_3$ compounds. In view of the characteristics of STEPT in fitting the Ru(dtc)$_3$ data, it was important to check if a fitting could be secured for the Fe(dtc)$_3$ data where the trigonal distortion was quite large. Theoretical susceptibility curves were calculated for D values up to ±5000 cm^{-1} with reasonable values for k and in no case was it possible to fit the data for Fe(Et2dtc)$_3$.

Figure 7[21] shows that the Fe((*n*-Bu)2dtc)$_3$ compound has a phase transition at ~140°K. This agrees with an earlier report.[12] As a consequence of this transition the magnetic data for this compound have to be fit in two sets and as can be seen the fittings are poor.

Unfortunately, correlation coefficients were not determined for the parameters of the various fittings in Table XIII. The parameters D and k are, obviously, used to describe the $^2T_{2g}$ states and are probably highly correlated. This can be shown by least-squares fittings wherein one of these two parameters (k or D) is held constant at one of selected values and the other is allowed to vary to obtain a fit. The energy separation ΔE is correlated to a lesser degree with k and D. As expected, for each compound the two fits with either positive or negative D yield comparable relative energies for the four electronic *states* (i.e., the three $^2T_{2g}$ Kramers doublets and the $^6A_{1g}$ state). In Table XIII we give ΔE_{eff} values, where ΔE_{eff} is the energy separation between the lowest Kramers doublet from the $^2T_{2g}$ state and the barycenter of the $^6A_{1g}$ state weighted by the vibrational partition factor. It is interesting that this ΔE_{eff} parallels the energy separation (E) obtained by Ewald et al.[12]

Infrared Data. An investigation of the variable-temperature infrared spectra of the Fe(dtc)$_3$ compounds could provide the answer to the following three questions: (1) Is the vibrational partition factor, as implicated by the susceptibility fitting, properly formulated per the observed FeS_6 vibrational frequencies? (2) Are there any indications of shifts in ir bands as a function of temperature as the temperature-dependent ΔE model would seemingly require? (3) Are distinct features seen for the $^6A_1$ and $^2T_2$ states of the "intermediate-spin" compounds?

There have been several studies of the variable-temperature infrared characteristics of spin-equilibria systems. Baker and Long[44] reported distinct variable-temperature high-spin and low-spin features for the C–N stretching region and Takemoto and Hutchinson[45] for the Fe–N far-ir stretching region for Fe(phen)$_2$X$_2$, X$^-$ = NCS$^-$ and NCSe$^-$, and Fe(bpy)$_2$(NCS)$_2$. The analysis of the susceptibility of these compounds, where there is an abrupt change in μ_{eff}, points to a temperature-dependent energy separation $\Delta E = E(^5T_2) - E(^1A_1)$ which gradually increases upon lowering the temperature to the phase transition temperature, rapidly increases over a 2 K range, continues to increase to a maximum, and then decreases. If this is the case, the high-spin ν(Fe–N) and ν(NCS) frequencies should change within the high-spin region and the low-spin ν(Fe–N) and ν(NCS) frequencies should also change within the low-spin region. Thus, if the Fe(II) atom experiences a variable-temperature crystal field, the various bond strengths and to a certain degree the stretching frequencies should change with temperature. However, the careful ir measurements of Sorai and Seki show that these frequencies are all constant with changing temperature.[14] This conflicts with the variable energy separation interpretation, and, instead, Sorai and Seki explained the "abrupt" nature of this $^5T_2$–$^1A_1$ equilibrium in terms of a *constant* ΔE *and* a phonon-coupled first-order phase transition. Thus, the abruptness grows out of an appreciable entropy contribution to the free energy and this ΔS is a reflection of large changes in vibrational frequencies in going from high spin to low spin.

Another spin-equilibrium system studied with ir methods is Co(NNP)(NCS)$_2$ where NNP is Et$_2$N(CH$_2$)$_2$NH(CH$_2$)$_2$PPh$_2$.[46] This compound shows a gradual change in μ_{eff} with temperature. There are distinct high-spin and low-spin ν(NCS) bands and the *positions* of both are a function of temperature, implicating a variable-temperature energy separation $\Delta E = E(^4T_{1g}) - E(^2E_g)$. A very recent report[47] of variable-temperature and -pressure studies of the far-ir (i.e., Co–N, etc.) region shows complex changes of the ir data with temperature and it is difficult to tell if the cobalt–ligand frequencies are a function of temperature.

Some preliminary variable-temperature ir data for certain Fe(dtc)$_3$ compounds have been reported by Ewald et al.[12] They assigned the asymmetric Co–S band for Co(Me2dtc)$_3$ as a band at 360 cm^{-1} by comparison with data[13] for tris(dimethyldiselenocarbamato)cobalt. Likewise, they assigned one or two bands in the 300–400-cm^{-1} region as Fe–S stretching bands for the Fe(dtc)$_3$ compounds. Our work adds to this previous work by the larger number of Fe(dtc)$_3$ and related compounds studied and the greatly increased resolution obtained at lower temperatures.

Nakamoto et al.[48] analyzed the ir spectra for M(S$_2$CNH$_2$)$_2$ (M = Ni, Pd, Pt) in terms of an approximation involving a Urey–Bradley force field for a 1:1 (metal:ligand) complex where the M(dtc)$_3$ moiety is treated in C_{2v} symmetry. More recent and accurate normal-coordinate analyses have treated the compounds as 1:2 complexes in D_{2h} symmetry.[49,50] Jensen et al.[49] assigned a b_{1u} largely ν_s(NiS) band at 388 cm^{-1} and a b_{3u} largely ν_{as}(NiS) band at 376 cm^{-1} for Ni(Me2dtc)$_2$. In the 300–400-cm^{-1} region, a band at 301 cm^{-1} was assigned

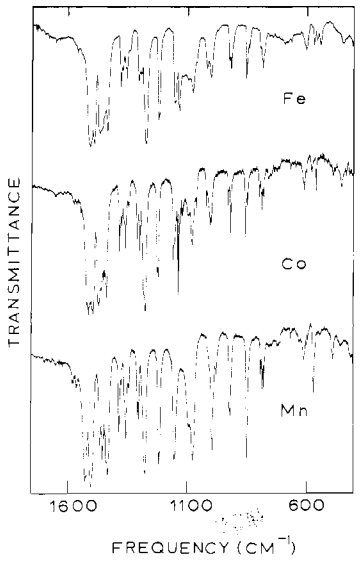

Figure 8. Infrared spectra (1700–400 cm^{-1}) of $M(Et_2dtc)_3$ pelleted in KBr with M = Fe, Co, and Mn run at ~30 K.

a mixing of the deformations δ(CNC) and δ_s(CSNi). On the other hand, Ojima et al.[50] without the added insight of deuteration and selenium analogues had assigned the largely ν_s(NiS) and ν_{as}(NiS) modes in the same region such that they are spaced by 75 cm^{-1}. In order for these two bands to be placed so far apart it is necessary, as was pointed out by Jensen et al., to introduce a relatively large interaction force constant in the generalized valence force field (GVFF).

There have been no normal-coordinate analyses on six-coordinate transition metal dithiocarbamates. We have collected 30–300 K infrared absorption data for tris(dithiocarbamate) complexes of Co(III), Fe(III), Ru(III), Cr(III), and Mn(III). Because single-crystal x-ray structures have been reported for $M(Et_2dtc)_3$ complexes where M = Co,[29] Fe,[28] Ru,[30] and Mn,[51] it is appropriate to look first at the 400–1600-cm^{-1} ir spectra of this series (run at ~30 K for the best resolution and to have the iron system in the lowest Kramers doublet); the spectra for the Co, Fe, and Mn compounds are reproduced in Figure 8. As expected from the x-ray structures, in this region the ir spectra of the Co and Fe species are largely identical. The isostructural $Ru(Et_2dtc)_3$ compound also gives an identical spectrum, as does the structurally uncharacterized Cr compound. In fact, only $Mn(Et_2dtc)_3$ in this series gives a spectrum unlike the others. The x-ray structure[51] of this compound indicates unequal Mn–S bond lengths. This is peculiar in that, as Figure 8 shows, the Mn spectrum has a "cleaner" appearance with less splitting of bands. One would have guessed that the Mn compound was of higher symmetry (at least at the low temperature). We have also found that for the other alkyl groups a comparison of ir spectra above ~400 cm^{-1} for different metal complexes (only one Mn complex was prepared) shows them to be reasonably superimposable. Generally, there is little effect, except resolution, of varying the temperature upon the ir spectra in the 4000–400-cm^{-1} region even for the $Fe(dtc)_3$ complexes which are "intermediate spin".

Figure 9 illustrates the very appreciable differences that occur in the 300–400-cm^{-1} region for $M(Et_2dtc)_3$ as the metal is changed. In the D_3 point group M–S stretching modes are expected with the symmetries $a_1 + a_2 + 2e$. Infrared-active modes include the a_2 and the two e symmetry modes. The spectrum of $Co(Et_2dtc)_3$ has good resolution (see Figure 9) and there appear to be three Co–S stretching bands at 376, 364, and 360 cm^{-1}. The two somewhat lower intensity bands at 392 and 404 cm^{-1} are not metal dependent and, in fact, a band in this region is seen in the spectrum of $Na(Et_2dtc)$. The

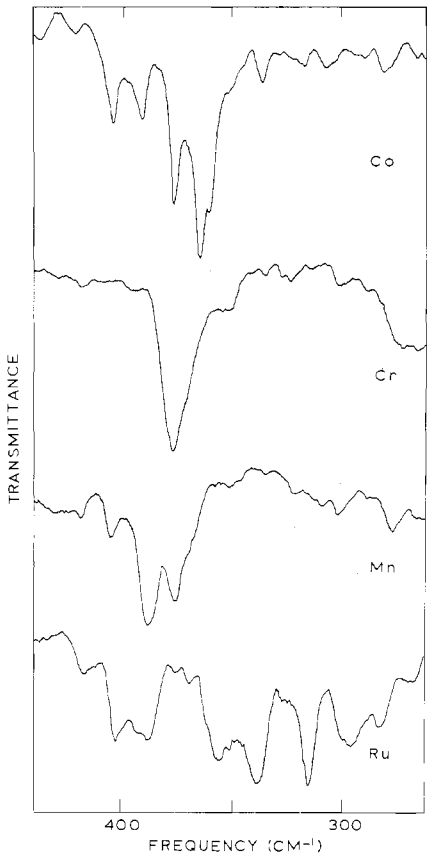

Figure 9. Infrared spectra (450–250 cm^{-1}) of $M(Et_2dtc)_3$ pelleted in CsI with M = Co, Cr, Mn, and Ru.

three Co–S bands could be assigned to the three ($a_2 + 2e$) infrared-active modes predicted. Three Co–S stretching bands (370, 367, 355 cm^{-1}) are also seen for $Co(Me_2dtc)_3$. Lower resolution spectra were obtained for the $Co((n\text{-}Pr)_2dtc)_3$ and $Co((i\text{-}Bu)_2dtc)_3$ systems; however, in all cases the Co–S stretching bands are found in the same ~20-cm^{-1} region, implying small interaction force constants in the GVFF approximation. These Co(III) compounds have $^1A_1$ ground states.

The $Cr(dtc)_3$ compounds also have orbitally nondegenerate ground states (i.e., $^4A_2$). The Cr–S stretching modes for $Cr(Et_2dtc)_3$ are found in the broad band at 377 cm^{-1}. Figure 10[21] shows the far-infrared characteristics of the only totally high-spin ($^6A_1$) ferric complex studied, that is, $Fe((pyrr)dtc)_3$. This orbitally nondegenerate system also shows M–S infrared-active stretching bands (324 and 334 cm^{-1}) extending over a narrow range. In this same regard it can be seen (Figure 9) that $Mn(Et_2dtc)_3$ appears to have only two relatively closely spaced bands (388 and 376 cm^{-1}). The band at 405 cm^{-1} is probably one of the aforementioned ligand-based bands. This Mn(III) complex has a ^5E_g (O_h symmetry) ground state.

Unlike the above complexes, the $Ru(dtc)_3$ complexes have ir spectra with many Ru–S stretching bands encompassing a relatively large range. For example, the spectrum of $Ru(Et_2dtc)_3$ (see Figure 9) shows bands at 376, 356, 339, 316, and 297 cm^{-1}. Under the influence of appreciable trigonal distortion and spin–orbital interaction the $^2T_{2g}$ state is split into three widely spaced Kramers doublets and there is only appreciable thermal population in the lowest of these. Perhaps there are relatively large interaction force constants in the $Ru(dtc)_3$ molecules. This could reflect a greater coupling of vibrational and electronic wave functions for these distorted $^2T_{2g}$ systems. At temperatures approaching ~30 K the "intermediate-spin" $Fe(dtc)_3$ species are also in the lowest

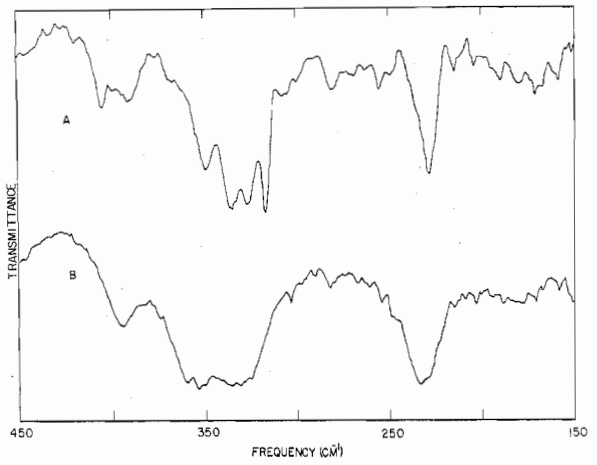

Figure 11. Infrared spectra (450–150 cm^{-1}) of $Fe(Et_2dtc)_3$ pelleted in CsI at two different temperatures: A, 30 K; B, room temperature.

energy Kramers doublet resultant from the distorted $^2T_{2g}$ state. The variable-temperature far-ir characteristics of $Fe(Et_2dtc)_3$ are given in Figure 11; four Fe–S stretching bands with appreciable intensity are seen at 346, 335, 326, and 316 cm^{-1}. For the diethyl R group, the Fe(III) species has a somewhat narrower range of M–S stretching bands than the Ru(III) species. This multiplet wide-range character is quite general for the $Fe(dtc)_3$ species at low temperature as can be seen in Figure 12[21] which compares the spectra of the Fe^{III}- and $Co^{III}((i\text{-}Pr)_2dtc)_3$ compounds. At this point, we can only speculate that the wide-ranging M–S stretching band region for these distorted, spin–orbital split $^2T_{2g}$ systems is a reflection of the greater orbital degeneracy of the $^2T_{2g}$ state or more specifically the greater vibrational–electronic coupling leading to larger interaction force constants.

The "intermediate-spin" $Fe(dtc)_3$ systems do appear to give separate Fe–S stretching bands for the $^6A_1$ and $^2T_2$ levels. A close inspection of Figure 11 shows that a band system centered at ~360 cm^{-1} loses intensity as the lower energy multiplet for the low-spin ground state grows in at low temperature. This can more easily be seen in the solid-state spectra of some of the other $Fe(dtc)_3$ species, for example, those for $Fe(Me_2dtc)_3$ and $Fe((n\text{-}Pr)_2dtc)_3$ depicted in Figure 13. The room-temperature tracing (top) for the dimethyl compound shows three broad-band systems, one for the high-spin level at 360 cm^{-1} and the other two for the low-spin level at 334 and 305 cm^{-1}. As the temperature is lowered (from top to bottom tracing) the lower energy band system at 336 cm^{-1} grows in at the expense of the band at 360 cm^{-1}. The band at ~305 cm^{-1} also gains in intensity. Figure 13 also shows that the same behavior is seen for $Fe((n\text{-}Pr)_2dtc)_3$. Because there are distinct bands reflecting the thermal populations in the two spin states, it is concluded that the spin-flipping rate is less than the vibrational time scale, that is, less than ~10^{13} sec^{-1}. The rate is also faster than the ^{57}Fe Mössbauer time scale, i.e., faster than ~10^7 sec^{-1}. In the EPR section the rate will be more closely bracketed.

One anomaly remains to be explained. The "intermediate-spin" $Fe(dtc)_3$ systems that we investigated with variable-temperature ir data all have their high-spin Fe–S stretching bands at *higher* energy than the low-spin bands. This is opposite to what is seen for $Fe(phen)_2X_2$, $X^- = NCS^-$ and $NCSe^-$, and $Fe(bpy)_2(NCS)_2$ where the high-spin Fe–N and C–N stretching bands are at *lower* energy than those for the low-spin complex. Even further, it is peculiar that the Fe–S band system for the high-spin $Fe(pyrr)dtc)_3$ species is at lower energy that the "high-spin" band system for the "intermediate-spin" compounds.

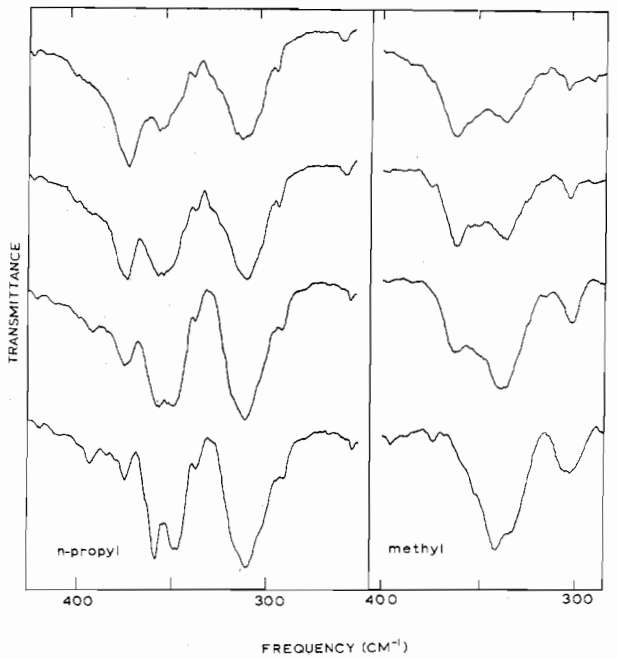

Figure 13. Infrared spectra of $Fe((n\text{-}Pr)_2dtc)_3$ and $Fe(Me_2dtc)_3$ pelleted in CsI. The temperature at which the spectra were recorded decreases successively from room temperature for the top scan to 30 K for the bottom scan.

One possible explanation is that the high-temperature band does not result from the high-spin state but is a reflection of population in the second Kramers doublet from the $^2T_{2g}$ level. However, if this is the case, one wonders where the $^6A_1$ Fe–S stretching band system has gone, given the fact that the room-temperature μ_{eff} for some of the $Fe(dtc)_3$ species is quite large (~4–5 BM). The magnitude of spin–orbit and trigonal distortion in these complexes leads to little (<10%) population in the second $^2T_{2g}$ Kramers doublet and as such, the high-temperature band is clearly due to the $^6A_1$ level.

A second explanation for the small and low energy shift of Fe–S bands as the system changes from high-spin to low-spin character could be found in the vibronic nature of these species. The $Fe(dtc)_3$ $^2T_2$ state (or for that matter both the $^2T_2$ and the $^6A_1$ states) could be very vibronic and naive expectations as to changes in Fe–S stretching frequencies in going from high spin to low spin would not be met. The coupling of the electronic and vibrational wave functions in the covalent $Fe(dtc)_3$ complexes ($^2T_2$ state) could in some way lead to a lowering in energy of the $^2T_{2g}$ Fe–S stretching frequencies. In keeping with this, the $Fe(phen)_2X_2$ and $Fe(bpy)_2(NCS)_2$ species probably have less vibronic character. The $^6A_1$–$^2T_2$ spin equilibria tris(monothio-β-diketonato)iron(III) species probably also have less vibronic character than the $Fe(dtc)_3$ species. Figure 14 shows the variable-temperature infrared spectra for tris(1,3-diphenyl-1,3-diketopropanato)iron(III). As with the other systems there appear to be distinct iron–ligand bands for the high-spin and for the low-spin species; the high-spin band is at 370 cm^{-1} while the low-spin band appears at 390 cm^{-1}. It is interesting that, in this d^5 case, the high-spin band is at lower energy than the low-spin band; however, the difference is considerably less than the ~150-cm^{-1} difference seen for $Fe(phen)_2X_2$.

Detailed normal-coordinate analyses, employing isotopic substitution, deuteration, etc., are needed to firmly establish all of the above assignments of Fe–S stretching bands.

If the infrared-active Fe–S stretching bands for the low-spin state are at lower energy and if, as seems reasonable, the other Fe–S stretching and bending modes follow this trend, then the vibrational partition factor used in the susceptibility analysis

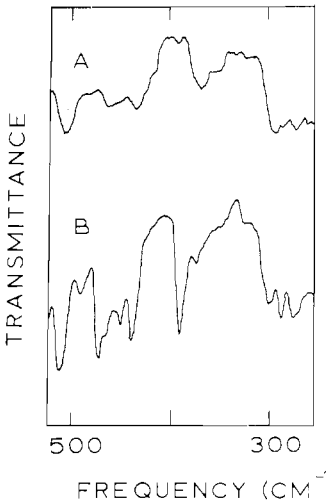

Figure 14. Infrared spectra (500–250 cm^{-1}) of tris(1,3-diphenyl-3-thioloprop-2-ene-1-one)iron(III) pelleted in KBr at two temperatures: A, room temperature; B, 30 K.

is *not* correct. In fact, the infrared frequencies change little from high- to low-spin state and as such the factor is approximately unity. The suggestion that ΔE is temperature dependent also can be countered by a close inspection of the temperature dependence of the positions of either the high-spin or low-spin Fe–S bands. However, it is clear from the susceptibility data that as the temperature is increased, a mechanism is needed to increase effectively the contribution of the $^6A_1$ state to the magnetism. We wish to suggest that a pseudo Jahn–Teller effect (i.e., vibronic coupling) is active in the $Fe(dtc)_3$ molecules. Ham has shown[52] that, for an octahedral complex experiencing trigonal distortion and spin–orbital interactions, vibronic coupling off-diagonal matrix elements effectively attenuate both the trigonal distortion and spin–orbital interactions. In our case, it is required somehow that at the higher temperatures an increased vibronic coupling would decrease the splitting (DS_z^2 and $\lambda L \cdot S$) in the $^2T_2$ manifold and the $^6A_1$ state would then in effect be closer in energy to the ground-state Kramers doublet of the $^2T_2$ state. However, such is *not* the case if the Ham effect is only operational within the $^2T_2$ manifold. The Ham effect corresponds to the specific limit of electronic–vibronic interaction wherein vibrations are included in the zero-order wave function and then the in-state electronic terms are added as perturbations. If only the Ham effect were operational within the $^2T_2$ manifold, the increased vibrational wave function overlap (in higher energy vibronic levels) at higher temperatures would lead to less attenuation and, thus, the splitting of the $^2T_2$ manifold would increase with increasing temperature. Perhaps a very complicated vibronic coupling within and between the $^2T_2$ and $^6A_1$ manifolds with many vibrational quanta is present and would explain the temperature dependence of the magnetic susceptibility. Obviously, we do not have the data at hand to warrant (or check) such a calculation. Potentially, EPR could give some of the necessary data and in the next section we turn to EPR to show that indeed the EPR observables do not fit a simple model.

Electron Paramagnetic Resonance. The EPR characteristics expected for a high-spin d^5 system have been discussed in many papers.[53] An intense $g \simeq 4.3$ signal is seen for an octahedrally coordinated Fe^{3+} ion (e.g., $Fe(H_2O)_6^{3+}$); several additional weak features are also seen depending on conditions. The positions of the various transitions can be used to evaluate zero-field parameters.

Both Q-band and X-band EPR spectra were obtained for high-spin $Fe((pyrr)dtc)_3$ under various conditions as can be seen in Figure 15. The lowest temperature available on our

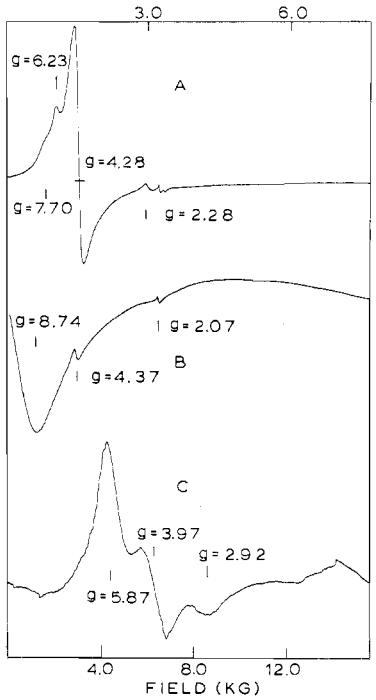

Figure 15. EPR spectra of $Fe((pyrr)dtc)_3$ where A is the X-band chloroform glass spectrum at 12 K, B is the X-band solid spectrum at 12 K, and C is the Q-band solid spectrum at 4.2 K. The top magnet field indicators are for the top two spectra.

X-band spectrometer is 12 K and under these conditions a solid sample gave a broad feature with a minimum at $g = 8.74$ in addition to two weaker and sharper peaks at $g = 4.37$ and 2.07 (tracing B in Figure 15). The very recent work of Sinn[33] clearly points to the presence of an intramolecular antiferromagnetic exchange interaction in this compound and perhaps this X-band spectrum reflects an exchange field at or near the X-band frequency. Q-Band measurements (tracing C in Figure 15) on the same solid sample at 4.2 K (direct immersion in liquid helium) give a spectrum with three relatively sharp features at $g = 5.87$, 3.97, and 2.92. Previously it has been noted[54a] that EPR line widths are influenced by electron-exchange interactions. If the exchange frequency is intermediate between the X- and Q-band frequencies, then the so-called "10/3 effect" is expected.[54b] Magnetic dilution (chloroform glass maintained at 12 K) also gives an X-band spectrum (tracing A in Figure 15) with relatively sharp $g = 6.23$ and 4.28 peaks with a shouldering feature at $g = 7.70$ and a weak peak at $g = 2.28$. As is shown in Table XIV, calculation of EPR transitions for such a $^6A_1$ species with the B_4^0, B_4^3, and B_2^0 parameters obtained in the susceptibility fitting gives expected peaks at $g = \simeq 4.0$, 6.1, and 3.0. The $g = 4.0$ signal arises from parallel field transitions within both the $\pm 5/2$ and $\pm 1/2$ Kramers doublets and from past experience would be expected to be most intense. The $g = 6.1$ value is associated with parallel field transitions within the $\pm 3/2$ doublet and the $g = 3.0$ value with perpendicular field transitions within the $\pm 5/2$ and $\pm 1/2$ doublets. The zero-field parameters were obtained for a magnetically concentrated sample and because the exchange frequency is probably less than the Q-band frequency, the 4.2 K Q-band spectrum for the magnetically concentrated sample gives the better agreement with the calculated g values. For the present, these $Fe((pyrr)dtc)_3$ spectra will serve the purpose of indicating signal patterns expected for such a high-spin system. It must be noted that weak $g = 2.0$–2.2 signals are seen for Cu^{2+} impurities, and at low temperatures, as would be expected, these signals are susceptible to power saturation.

Bleaney and O'Brien[55] have discussed the EPR for a d^5 $^2T_2$

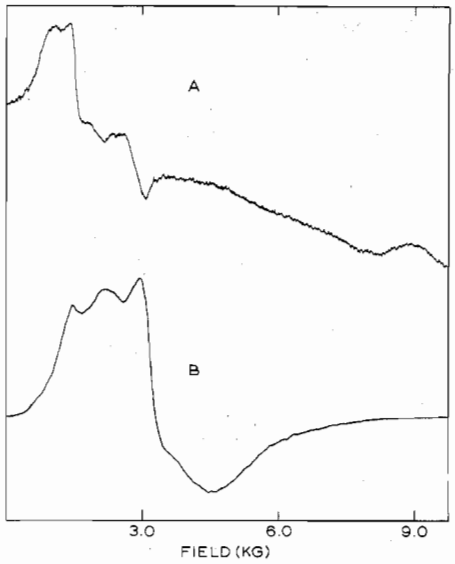

Figure 16. X-Band chloroform glass EPR spectra of $Fe(Et_2dtc)_3$: A, 85 K; B, 12 K.

ground state. Previous workers have studied the EPR of the $Fe(dtc)_3$ systems. Garif'yanov et al.[56] were not able to obtain an EPR signal for $Fe(Et_2dtc)_3$ from 350 to 4.2 K. Hill et al.[57] reported the EPR at 4.2 K for $Fe(Me_2dtc)_3$ doped into $Co(Me_2dtc)_3$ and obtained a relatively isotropic signal with $g_1 = 2.111$, $g_2 = 2.076$, and $g_3 = 2.015$. These workers did not mention in their paper to what degree the cobalt substrate was made "copper-free".[58] In the analysis of their data Hill et al. obtained a relatively small distortion parameter, while DeSimone's reanalysis gave a large distortion parameter analogous to what he found for $Ru(Et_2dtc)_3$. Recently workers have found signals similar to those reported by Hill et al. for $Mn(dtc)_3$ and they attributed the signals for both the Fe(III) and Mn(III) complexes to a metal–sulfur complex with the unpaired electron on the sulfur.[59] In spite of the difficulty previous workers had in obtaining $Fe(dtc)_3$ EPR signals, Flick and Gelerinter[60] recently reported the results of a variable-temperature (down to liquid nitrogen) EPR study of two $Fe(dtc)_3$ compounds for which they were able to obtain EPR signals for the magnetically concentrated solids at room temperature. It is our experience that the two compounds these workers studied are two of the $Fe(dtc)_3$ compounds which are the hardest to purify.

We could not see EPR signals for any of the $Fe(dtc)_3$ compounds at room temperature, including $Fe((n\text{-}Bu)_2dtc)_3$, which Flick and Gelerinter studied. In fact, it was only possible to see EPR signals for the magnetically concentrated solids at temperatures approaching 4.2 K. Figure 16 shows the relatively typical behavior of $Fe(Et_2dtc)_3$ in a $CHCl_3$ glass as a function of temperature. The ~85 K X-band spectrum (tracing A) shows two signals at $g = 6.5$ and 4.3 and a somewhat weaker derivative at $g \simeq 2.0$. From studying various $Fe(dtc)_3$ compounds in $CHCl_3$ glasses (freshly prepared and at later times) and doped in "copper-free" $Co(dtc)_3$, we believe that the $g \simeq 2.0$ signal at 85 K is due to a small copper impurity in $Fe(dtc)_3$. In this respect it would be interesting to know if the signal obtained by Hill et al. for $Fe(Me_2dtc)_3$ was not largely due to copper.[58] As the temperature of the $CHCl_3$ glass of $Fe(Et_2dtc)_3$ is lowered, the $g \simeq 4.3$ signal appears to lose intensity as new signals appear in the range of $g = 2.0$ to $g = 4.0$. The 12 K X-band $CHCl_3$ glass spectrum is shown in Figure 16 (tracing B). Features are seen at $g = 4.36$, 3.26, and ~1.83. The $g = 4.36$ peak appears as a shoulder and is not associated with a small residual $^6A_1$ population, because there is negligible $^6A_1$ population at 12 K. This weak signal is due to a combination

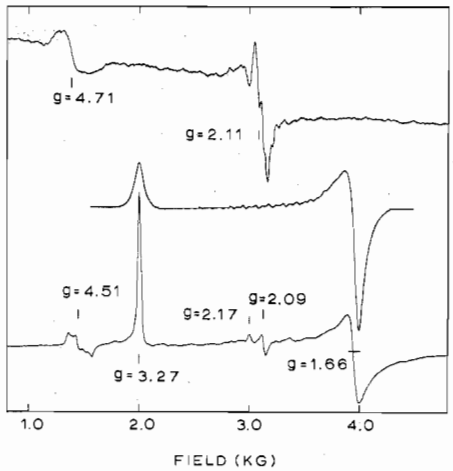

Figure 17. X-Band EPR spectra of 1% $Fe(Me_2dtc)_3$ doped into $Co(Me_2dtc)_3$. The top scan is at 85 K, the bottom scan is at 12 K, and the intermediate scan is a computer simulation with $g_\parallel = 3.27$ and $g_\perp = 1.64$.

of cavity contamination and perhaps some Fe^{3+} decomposition species resultant from the $CHCl_3$ solution. At 12 K Cu^{2+} signals would normally be relatively easy to saturate; our low-temperature spectra are run at large microwave power values and occasionally sharp power-dependent Cu^{2+} signals are seen. Thus, the $g = 3.27$ and ~1.83 signals are from the ground-state Kramers doublet of the $^2T_2$ state.

Similar types of temperature dependencies are seen for the other intermediate-spin $Fe(dtc)_3$ compounds. A few compounds were doped into "Cu-free" $Co(dtc)_3$ hosts, and, as Figure 17 shows for a sample of 1% $Fe(Me_2dtc)_3$ doped into $Co(Me_2dtc)_3$, there is a similar temperature dependence. Again, at ~85 K there is a $g = 4.71$ signal associated with $^6A_1$ population and a complicated signal at $g = 2.11$, largely due to Cu^{2+} impurity. Lowering the temperature to 12 K gives rise to two new peaks, one at $g = 3.27$ and another at $g = 1.66$. It is difficult to assign these new peaks to any other state than the ground-state Kramers doublet. A computer simulation with $g_\parallel = 3.27$ and $g_\perp = 1.64$ is also shown in Figure 17. The EPR results for doped samples of some of the other compounds are summarized in Table XIV.

The appearance of distinct features for what appears to be molecules in the $^6A_1$ and $^2T_2$ levels is informative insofar as the rate of spin flipping is concerned. In an analysis similar to that used for distinct peaks seen in an NMR chemical-exchange problem it is possible to conclude that the rate of spin flipping is less than approximately 10^{10} sec^{-1}. If this is correct, the rate of spin flipping for the $Fe(dtc)_3$ *solid* compounds is between ~10^7 and ~10^{10} sec^{-1}. To a large degree the faster rate of spin flipping in the $Fe(dtc)_3$ species compared to the $<10^7$-sec^{-1} rate for the $^6A_1$–$^2T_2$ tris(monothio-β-diketonato)ferric compounds is probably due to greater spin–orbital interaction. This interaction mixes the $^2T_2$ state with the $^4T_1$ state and $^6A_1$ with $^4T_1$. In summary, it is clear that the rate of spin flipping in $Fe(dtc)_3$ is great, but these compounds can still be described as "intermediate-spin" not as "mixed-spin" systems.

Returning to the suggestion that there is strong vibronic coupling present in the $^6A_1$ and $^2T_2$ levels of the $Fe(dtc)_3$ species, we next take a closer look at the EPR signals that have been assigned to the lowest energy $^2T_2$ Kramers doublet.

Figure 18[21] illustrates the 12 K X-band spectra obtained for four magnetically concentrated compounds (i.e., pure solids of the dimethyl, di-*n*-propyl, diethyl, and diisopropyl compounds). There are overall gross similarities from one spectrum to another; however, the marked differences clearly eliminate the possibility of the spectra being totally due to a

Table XIV. Experimental and Calculated g Values

Compd	X band 85 K Doped	X band 85 K Glass	X band 12 K Doped	X band 12 K Glass	X band 12 K Solid	Q band 4.2 K Solid	Calcd g values $^6A_1$	Calcd g values $^2T_2$
$Fe((pyrr)dtc)_3$	8.13	7.70	5.71	7.70	8.74	5.87	6.10	
	5.66	6.23	4.38	6.23	4.37	3.97	4.04	
	4.25	4.28	2.79	4.28	2.07	2.92	2.97	
	2.03	2.00	2.00	2.00			2.91	
$Fe(Et_2dtc)_3$	4.34	6.49		4.36	4.09	3.24	*c*	$g_\parallel = -0.69, g_\perp = -1.65$[a]
	2.04	4.33		3.27	3.27	1.81		$g_\parallel = -2.79, g_\perp = -0.48$[b]
				1.83	2.14			
$Fe((i\text{-}Pr)_2dtc)_3$	4.11	3.87	4.50	4.64	2.06	2.86	*c*	$g_\parallel = -0.53, g_\perp = -1.56$[a]
	2.01	2.05	3.21	3.22		2.07		$g_\parallel = -2.46, g_\perp = -0.36$[b]
			2.18	2.10				
			2.08					
$Fe((n\text{-}Pr)_2dtc)_3$	4.33	3.91		4.39	3.16	3.17	*c*	$g_\parallel = -1.31, g_\perp = -2.46$[a]
	2.03	2.07		3.09	1.83	2.15		$g_\parallel = -3.72, g_\perp = -0.98$[b]
				2.18	1.48	1.83		
					1.22			
$Fe(Me_2dtc)_3$	4.71	4.39	4.51	4.56	Broad	Broad	*c*	$g_\parallel = -0.99, g_\perp = -2.04$[a]
	2.11	2.06	3.27	3.30	peak	peak		$g_\parallel = -3.02, g_\perp = -0.83$[b]
			2.17	1.85				
			2.09					
			1.66					

[a] g values calculated from equations given in the text for an axial $^2T_2$ level using the parameters determined for the susceptibility fits with a temperature independent δ and $Q = 2.62$ at 296 K for the fitting model with $D > 0$. These g values are for EPR transitions in the lowest Kramers doublet only. [b] g values calculated as in footnote *a* from the parameters determined for the susceptibility fits with a temperature-independent δ and $Q = 2.62$ at 296 K for the fitting model with $D < 0$. [c] The calculated g values for the $^6A_1$ level are the same as those calculated for $Fe((pyrr)dtc)_3$.

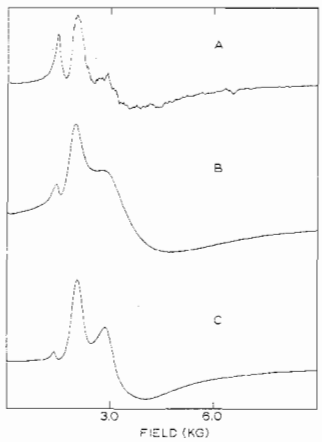

Figure 19. X-Band chloroform glass EPR spectra at 12 K: A, $Fe((n\text{-}Pr)_2dtc)_3$; B, $Fe(Me_2dtc)_3$; C, $Fe((i\text{-}Pr)_2dtc)_3$.

common impurity or decomposition product. In comparison to the $CHCl_3$ glass spectra (vide infra) there are no $g \simeq 4.0$ signals to be seen in these 12 K pure solid spectra. In each case, there is a relatively intense signal peaking in the range of $g = 3.2$–3.3. In two of the cases signals with g values less than 2.0 are seen. The sharp spike seen for $Fe((i\text{-}Pr)_2dtc)_3$ is typical of a Cu^{2+} impurity. The Cu^{2+} signal is well resolved and its intensity is quite sensitive to the microwave power setting. The signals for $Fe(Me_2dtc)_3$ and $Fe((i\text{-}Pr)_2dtc)_3$ are relatively broad; the signal is by far the broadest for the dimethyl compound.

Improved resolution results (see Figures 16 and 19) when these same four $Fe(dtc)_3$ compounds are studied as freshly prepared $CHCl_3$ glasses at 12 K with the X-band spectrometer. Now, both spectra for the methyl and isopropyl compounds are resolved. For the three compounds in Figure 19, there is clearly visible in each case a signal at $g = 4.4$–4.6 as we saw for the glass of $Fe(Et_2dtc)_3$. As we mentioned above, this is probably due to an impurity.

Unfortunately, it was not possible with our instrumentation to run 4.2 K $CHCl_3$ glasses at Q-band frequencies. Nevertheless, an improvement from the 12 K X-band spectra for the pure solids is seen in Figure 20, which shows the 4.2 K Q-band spectra for the same pure compounds. Particularly, it seems that no $g \simeq 4.5$ signal is seen for any of the four compounds. The $Fe(Me_2dtc)_3$ signal (tracing C in Figure 20) is broad perhaps due to intermolecular electron exchange. The g values of signals seen in Figures 16–19 are summarized in

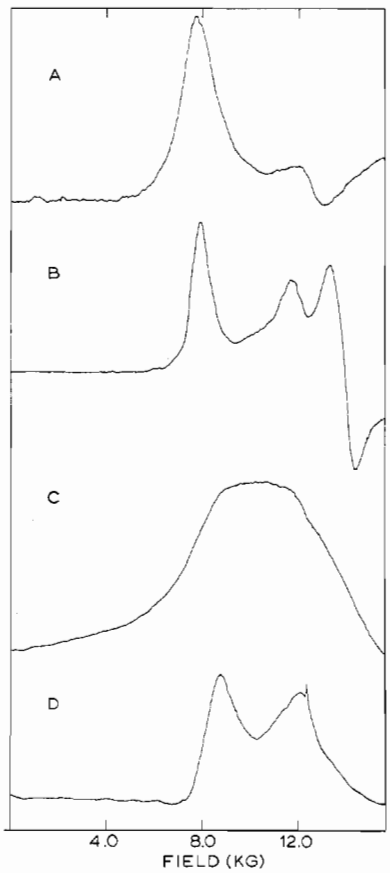

Figure 20. Q-Band EPR spectra of solid compounds at 4.2 K: A, $Fe(Et_2dtc)_3$; B, $Fe((n\text{-}Pr)_2dtc)_3$; C, $Fe(Me_2dtc)_3$; D, $Fe((i\text{-}Pr)_2dtc)_3$.

Table XIV. The parameters (k and D) obtained from the susceptibility fittings were used to calculate the $g\parallel$ and $g\perp$ values expected for the ground-state ($^2T_2$) Kramers doublets and these are also listed in Table XIV. It is seen, using a $^6A_1$–$^2T_2$ equilibrium *with* a vibrational partition factor, that for the fittings with $D > 0$, a $g\parallel$ value less than 1.5 and a $g\perp$ value between 1.5 and 2.5 are expected. For the fittings with $D < 0$, a $g\parallel$ value between 2.5 and 3.8 and a $g\perp$ value less than 1 are predicted. The simulation of the doped $Fe(Me_2dtc)_3$ EPR with $g\parallel = 3.27$ and $g\perp = 1.64$ indicates that the fits with negative D values are more reasonable since they predict correctly $g\parallel > g\perp$. However, the exact experimental values are not in agreement with calculated g values except for unreasonable parameter values. For example $g\parallel = 3.2$ and $g\perp = 1.9$ values are predicted for $D/\xi = -0.5$ and $k = 1.3$. A k value much greater than 1 is not reasonable.

The discrepancy between the experimental and calculated g values for the lowest energy $^2T_2$ Kramers doublet again points to the possible importance of pseudo Jahn–Teller effects for these $Fe(dtc)_3$ compounds. Ammeter and Swalen[61] have correlated the experimental g values found for the lowest Kramers doublet of the cobaltocene molecule with theoretical g value equations which incorporate effects due to vibronic coupling between the two lowest Kramers doublets. For the ferric dithiocarbamates the Fe–S stretching modes have the correct symmetry to mix vibronically the various Kramers doublets. As mentioned earlier, the pseudo Jahn–Teller effect may also be important in explaining the unexpected position of the low-spin Fe–S stretching bands. Detailed theoretical and experimental work (e.g., EPR on doped single crystals over the 4.2–50 K range) is needed to substantiate the proposal that the pseudo Jahn–Teller effect is important for the ferric dithiocarbamates.

Conclusion

The observation of distinct EPR signals for both the $^6A_1$ and $^2T_2$ levels in the $Fe(dtc)_3$ compounds provides an upper limit of $\sim 10^{10}$ sec^{-1} for the spin flipping. Distinct $^6A_1$ and $^2T_2$ bands are also seen in the ir spectra; identification is possible because of temperature dependencies. The second important conclusion in this work bears on the probable vibronic nature of the total $^6A_1$–$^2T_2$ manifold. From ir peak positions and g values for the ground-state Kramers doublet, it is indicated that the previously used vibrational partition function and variable-energy approaches should be supplanted in these $Fe(dtc)_3$ compounds by detailed considerations of the vibronic nature of the systems. Other work is called for, work such as doped single-crystal EPR measurements in the ~4–50 K region.

Acknowledgment. We are grateful for partial funding of this research by National Institutes of Health Grant HL 13652. The Varian EPR spectrometers were purchased, in part, with a National Science Foundation departmental grant.

Registry No. $Fe(Me_2dtc)_3$, 14484-64-1; $Co(Me_2dtc)_3$, 23677-76-1; $Ru(Me_2dtc)_3$, 43190-67-6; $Fe(Et_2dtc)_3$, 13963-59-2; $Co(Et_2dtc)_3$, 13963-60-5; $Ru(Et_2dtc)_3$, 31656-15-2; $Mn(Et_2dtc)_3$, 15740-71-3; $Cr(Et_2dtc)_3$, 18898-57-2; $Fe((n\text{-}Pr)_2dtc)_3$, 15407-44-0; $Co((n\text{-}Pr)_2dtc)_3$, 28459-60-1; $Ru((n\text{-}Pr)_2dtc)_3$, 57527-42-1; $Fe((i\text{-}Pr)_2dtc)_3$, 15280-39-4; $Co((i\text{-}Pr)_2dtc)_3$, 24412-36-0; $Fe((allyl)_2dtc)_3$, 36759-15-6; $Fe((n\text{-}Bu)_2dtc)_3$, 14526-32-0; $Co((n\text{-}Bu)_2dtc)_3$, 28090-32-6; $Fe((i\text{-}Bu)_2dtc)_3$, 19543-96-5; $Co((i\text{-}Bu)_2dtc)_3$, 28090-33-7; $Fe((n\text{-pentyl})_2dtc)_3$, 23674-37-5; $Fe((n\text{-}Hx)_2dtc)_3$, 23674-38-6; $Fe((morph)dtc)_3$, 14285-01-9; $Co((morph)dtc)_3$, 27796-33-4; $Fe((pyrr)dtc)_3$, 21288-86-8; $Co((pyrr)dtc)_3$, 24412-38-2; $Ru((pyrr)dtc)_3$, 57527-43-2; tris(1,3-diphenyl-3-thioloprop-2-ene-1-one)iron(III), 16786-67-7.

Supplementary Material Available: Tables I (analytical data) and II–XII (experimental and theoretical susceptibility data) and Figures 5 (the temperature dependence of μ_{eff} for the diallyl, di-n-propyl, and diisopropyl compounds), 7 (μ_{eff} vs. temperature for the diisobutyl and di-n-pentyl compounds), 10 (430–200-cm^{-1} ir of pyrrolidyl compound at two temperatures), 12 (comparison of 430–150-cm^{-1} ir spectra for cobalt and iron diisopropyl compounds), and 18 (X-band EPR spectra of the pure solids of four compounds at 12 K) (20 pages). Ordering information is given on any current masthead page.

References and Notes

(1) NSF traineeship, 1970–1974.
(2) Camille and Henry Dreyfus Fellow, 1972–1977.
(3) L. Cambi and A. Cagnasso, *Atti. Accad. Naz. Lincei*, **13**, 809 (1931); L. Cambi and L. Szego, *Ber. Dtsch. Chem. Ges.*, **64**, 2591 (1931).
(4) R. L. Martin and A. H. White, *Transition Metal Chem.*, **4**, 113 (1968).
(5) E. K. Barefield, D. H. Busch, and S. M. Nelson, *Q. Rev., Chem. Soc.*, **22**, 457 (1968).
(6) E. König, *Coord. Chem. Rev.*, **3**, 471 (1968).
(7) L. Sacconi, *Pure Appl. Chem.*, **27**, 161 (1971).
(8) E. König, *Ber. Bunsenges. Phys. Chem.*, **76**, 975 (1972).
(9) A. H. White, E. Kokot, R. Roper, H. Waterman, and R. L. Martin, *Aust. J. Chem.*, **17**, 294 (1964).
(10) P. C. Healy and E. Sinn, *Inorg. Chem.*, **14**, 109 (1975).
(11) M. A. Hoselton, L. J. Wilson, and R. S. Drago, *J. Am. Chem. Soc.*, **97**, 1722 (1975).
(12) A. H. Ewald, R. L. Martin, E. Sinn, and A. H. White, *Inorg. Chem.*, **8**, 1837 (1969).
(13) E. König and S. Kremer, *Theor. Chim. Acta*, **20**, 143 (1971).
(14) M. Sorai and S. Seki, *J. Phys. Chem. Solids*, **35**, 555 (1974).
(15) D. F. Wilson, P. L. Dulton, M. Erecinsha, J. G. Lindsay, and N. Sato, *Acc. Chem. Res.*, **5**, 234 (1972); I. Morishima and T. Jizaka, *J. Am. Chem. Soc.*, **96**, 5279 (1974).
(16) J. K. Beattie and R. J. West, *J. Am. Chem. Soc.*, **96**, 1933 (1974).
(17) P. B. Merrithew and P. G. Rasmussen, *Inorg. Chem.*, **11**, 325 (1972).
(18) G. Harris, *Theor. Chim. Acta*, **10**, 119, 155 (1968).
(19) M. M. Maltempo, *J. Chem. Phys.*, **61**, 2540 (1974).
(20) M. Cox, J. Darken, B. W. Fitzsimmons, A. W. Smith, L. F. Larkworthy, and K. A. Rogers, *J. Chem. Soc., Dalton Trans.*, 1192 (1972).
(21) Supplementary material.
(22) L. Compin, *Bull. Soc. Chim. Fr.*, 464 (1920).
(23) L. Malatesta, *Gazz. Chim. Ital.*, **68**, 194 (1938).
(24) J. Chatt, L. A. Duncanson, and L. M. Venanzi, *Suom. Kemistil. B*, **29**, 75 (1956).
(25) R. M. Golding, P. Healy, P. Newman, E. Sinn, W. C. Tennant, and A. H. White, *J. Chem. Phys.*, **52**, 3105 (1970).
(26) D. M. Duggan and D. N. Hendrickson, *Inorg. Chem.*, **13**, 2929 (1974).
(27) P. C. Healy and A. H. White, *Chem. Commun.*, 1446 (1971); *J. Chem. Soc., Dalton Trans.*, 1163 (1972).
(28) J. G. Leipoldt and P. Coppens, *Inorg. Chem.*, **12**, 2269 (1973).
(29) T. Brennan and I. Bernal, *J. Phys. Chem.*, **73**, 443 (1969).
(30) L. H. Pignolet, *Inorg. Chem.*, **13**, 2051 (1974).
(31) The spin–orbit interaction is gauged by $\lambda = -k\xi$, where λ is the spin–orbit coupling constant for the $^2T_2$ electronic state and the parameter ξ, a positive quantity, is the one-electron constant and k is the orbital reduction parameter.
(32) B. N. Figgis, *Trans. Faraday Soc.*, **57**, 198 (1961).
(33) E. J. Cukauskas, B. S. Deaver, Jr., and E. Sinn, *J. Chem. Soc., Chem. Commun.*, 698 (1974).
(34) R. E. DeSimone, *J. Am. Chem. Soc.*, **95**, 6238 (1973).
(35) A. K. Gregson and S. Mitra, *Chem. Phys. Lett.*, **3**, 392 (1969).
(36) J. C. Chandler, Program 66, Quantum Chemistry Program Exchange, Indiana University, Bloomington, Ind.
(37) The data in Figure 1 were fit in the following way using the simplex minimization computer program STEPT. Zeeman interaction matrix terms were added to the spin–orbit and trigonal distortion terms for the two 6×6 Hamiltonian matrices (parallel and perpendicular magnetic fields) for such an axial $^2T_2$ system. The energies of the various levels were calculated at each temperature as a function of magnetic field (parallel and perpendicular orientations) by computer diagonalization. The average susceptibility [$\chi_{av} = {}^1/_3(\chi\parallel + 2\chi\perp)$] is calculated as a Boltzmann-weighted average of the magnetic moments ($\mu = -\partial E/\partial H$, evaluated as the slope of the energy of a given level at 15.0 kG) for the various energy levels. Thus, the program STEPT systematically varies the parameters used in a fitting in conjunction with exact matrix diagonalizations for χ_{av} evaluations. The function minimized was CHISQ = $\sum_{i=1}^{n}[\chi_i(\text{exptl}) - \chi_i(\text{calcd})]^2$ and the "standard error" indicator was taken as SE = $\{\sum_{i=1}^{n}[\mu_{eff}{}^i(\text{obsd}) - \mu_{eff}{}^i(\text{calcd})]^2/(n-K)\}^{1/2}$, where n is the number of data points and K is the number of parameters.
(38) A. P. Ginsberg and M. E. Lines, *Inorg. Chem.*, **11**, 2289 (1972).
(39) J. A. Stanko, H. J. Peresie, R. A. Bernheim, R. Wang, and P. S. Wang, *Inorg. Chem.*, **12**, 634 (1973).
(40) B. N. Figgis and G. E. Toogood, *J. Chem. Soc., Dalton Trans.*, 2177 (1972).
(41) V. R. Marathe and S. Mitra, *Chem. Phys. Lett.*, **21**, 62 (1973).
(42) J. M. deLisle and R. M. Golding, *Proc. R. Soc. London, Ser. A*, **296**, 457 (1967).
(43) G. R. Hall, Ph.D. Thesis, University of Illinois, 1975.
(44) W. A. Baker, Jr., and G. J. Long, *Chem. Commun.*, 368 (1965).
(45) J. H. Takemoto and B. Hutchinson, *Inorg. Chem.*, **12**, 705 (1973).
(46) R. Morassi and L. Sacconi, *J. Am. Chem. Soc.*, **92**, 5241 (1970).
(47) L. Sacconi and J. R. Ferraro, *Inorg. Chim. Acta*, **9**, 49 (1974).

(48) K. Nakamoto, J. Fujita, R. Condrate, and Y. Morimoto, *J. Chem. Phys.*, **39**, 423 (1963).
(49) K. A. Jensen, B. M. Dahl, P. H. Nielsen, and G. Borch, *Acta Chem. Scand.*, **26**, 2241 (1972).
(50) I. Ojima, T. Onishi, T. Iwamoto, N. Inamoto, and K. Tamaru, *Inorg. Nucl. Chem. Lett.*, **6**, 65 (1970).
(51) P. C. Healy and A. H. White, *J. Chem. Soc., Dalton Trans.*, 1883 (1972).
(52) F. S. Ham, *Phys. Rev. A.*, **138**, 1727 (1965); F. S. Ham in "Electron Paramagnetic Resonance", by S. Geschwind, Ed., Plenum Press, New York, N.Y., 1972, Chapter 1.
(53) R. D. Dowsing and J. F. Gibson, *J. Chem. Phys.*, **50**, 294 (1969); H. H. Wickman, M. P. Klein, and D. A. Shirley, *ibid*, **42**, 2115 (1965); T. Castner, G. S. Newell, W. C. Holton, and C. P. Slichter, **32**, 668 (1960).
(54) (a) R. Scaringe and G. Kokoszka, *J. Chem. Phys.*, **60**, 40 (1974); (b) P. W. Anderson and P. R. Weiss, *Rev. Mod. Phys.*, **25**, 269 (1963).
(55) B. Bleaney and M. C. M. O'Brien, *Proc. Phys. Soc., London, Sect. B*, **69**, 1205 (1956).
(56) N. S. Garif'yanov, S. S. Kamenev, B. M. Kozyrev, and I. V. Ovichinnikov, *Dokl. Akad. Nauk. SSSR*, **177**, 880 (1967).
(57) R. Rickards, C. E. Johnson, and H. A. O. Hill, *J. Chem. Phys.*, **53**, 3118 (1970).
(58) However, a private communication with Dr. H. A. O. Hill informed us that, in fact, their cobalt substrate was relatively copper free and gave no copper EPR signal. Moreover, Dr. Hill suggested, and we concur, that copper was probably present in the iron sample and that this probably led to their copperlike EPR signal.
(59) R. M. Golding, E. Sinn, and W. C. Tennant, *J. Chem. Phys.*, **56**, 5296 (1972).
(60) C. Flick and E. Gelerinter, *Chem. Phys. Lett.*, **23**, 422 (1973).
(61) J. H. Ammeter and J. D. Swalen, *J. Chem. Phys.*, **57**, 678 (1972).

Contribution from the Department of Chemistry, The State University of New York at Buffalo, Buffalo, New York 14214, and the University of New Orleans, Lakefront, New Orleans, Louisiana 70122

Preparation, Characterization, Mössbauer Spectra, and Electron Spin Resonance Spectra of Iron(II) and Iron(III) Complexes of the Dithiolate Cyclopentadienedithiocarboxylate

ROBERT D. BEREMAN,*[1a] MARY L. GOOD,*[1b] BARBARA J. KALBACHER,[1a] and JOHN BUTTONE[1b]

Received August 18, 1975 AIC50617J

The preparation of tetraethylammonium salts of bis(cyclopentadienedithiocarboxalato)ferrate(II) and tris(cyclopentadienedithiocarboxalato)ferrate(III) is reported. Both complexes exhibit high-spin behavior. The Mössbauer spectrum of the iron(II) complex is characterized by IS = 0.69 mm/s (metallic iron reference) and ΔE_q = 4.52 mm/s at 78 K. The large quadrupole splitting is rationalized by the apparent five-coordination at the Fe(II) ion in the solid state. The observation of a temperature-independent magnetic moment in the iron(III) complex allows the placement of the cyclopentadienedithiocarboxylate ligand in the spectrochemical series of dithiolate ligands. The Mössbauer spectrum of the iron(III) complex is characterized by IS = 0.41 mm/s (broad singlet with Γ of 1.71 mm/s) at 78 K. The electron spin resonance spectrum of the iron(III) complex exhibits g = 9.30, 4.31, and 0.77, characteristic of a large zero-field splitting of the $^6S_{5/2}$ system.

Introduction

The tremendous interest which has been generated in the study of iron–sulfur enzymatic systems[2,3] makes the study of iron–sulfur complexes of varying oxidation states and chemical environments of particular importance. While a large body of work exists on iron(III) 1,2-dithiolene and 1,1-dithiolate complexes, the majority are low spin in nature. Iron(II) complexes are known but their occurrence is rare.[4] In particular, aliphatic and aromatic iron(II) dithiolates are unknown.[5] Our interest in the effect of the cyclopentadienedithiocarboxylate ($cpdt^{2-}$) ligand coupled with the large accumulation of knowledge on iron dithiolate complexes prompted our investigation of Fe–$cpdt^{2-}$ systems so that comparisons could be made.

Experimental Section

Materials. Acetonitrile was repeatedly distilled from phosphorus pentoxide. Anhydrous $FeBr_2$ and $FeCl_3$ were purchased from Research Organic-Inorganic Chemical Corp. Anhydrous $(C_2H_5)_4NCl$ and $(C_2H_5)_4NBr$ were obtained from Aldrich Chemical Co.

The disodium salt of cyclopentadienedithiocarboxylic acid, $Na_2S_2CC_5H_4$, was prepared as previously reported.[6]

$[(C_2H_5)_4N]_2Fe(C_5H_4CS_2)_2$. Typically, 0.613 g of $FeBr_2$ was dissolved in anhydrous degassed acetonitrile. The resulting solution was frozen and both 1.555 g of $Na_2S_2CC_5H_4$ and 1.138 g of $(C_2H_5)_4NBr$ were added. The resulting mixture was allowed to thaw slowly while stirring. After the resulting brown solution had stirred for 2 h at room temperature, NaBr was removed by filtration. The filtrate was reduced in volume under vacuum and the bright red product was removed by further filtration. Anal. Calcd for $[(C_2H_5)_4N]_2Fe(C_5H_4CS_2)_2$: C, 56.35; H, 8.11; N, 4.69. Found: C, 56.44, H, 8.03; N, 4.74.

$[(C_2H_5)_4N]_3Fe(C_5H_4CS_2)_3$. This air-sensitive brown complex was prepared in the same manner as the iron(II) complex above. Typical starting ratios were 0.7002 g of $FeCl_3$, 3.3233 g of $Na_2S_2CC_5H_4$, and 2.189 g of $(C_2H_5)_4NCl$. Anal. Calcd for $[(C_2H_5)_4N]_3Fe(C_5CS_2)_3$: C, 58.16; H, 8.31; N, 4.85; S, 22.18. Found: C, 57.65; H, 8.44; N, 4.66; S, 21.53.

Analysis. All analyses were carried out by Galbraith Laboratories, Inc., Knoxville, Tenn.

Methods. Reactions, filtrations, transfers, etc. were carried out in as rigorously anhydrous (nitrogen) an atmosphere as could be maintained employing Schlenk-tube techniques.[6] Both compounds of iron were *very* air sensitive and decomposed to a black material almost instantaneously when exposed to the atmosphere.

Magnetic Susceptibility Determinations. Magnetic susceptibilities were carried out on solid samples using the Gouy method and $Hg[Co(SCN)_4]$ as a calibrant. Pascal's constants were used to correct for diamagnetic contributions from the ligand, the cation, and the core electrons of the metal.[7] Measurements made at other than ambient room temperature employed a Dewar assembly and liquid nitrogen–solvent slushes or liquid nitrogen as coolant.

Spectroscopic Measurements. Mössbauer spectra were obtained using an Austin Science Associates, Inc., spectrometer equipped with a "fast data accumulation package" electronics system. A Nuclear Data Model 2200 multichannel analyzer was used for data collection and storage. Data were transmitted via a teletype terminal into a PDP-10 computer for data reduction. A least-squares fit, assuming Lorentzian line shapes, was performed for each spectrum. Velocity calibration was done by laser interferometry and all spectra were referenced to an iron foil standard with the midpoint of the iron spectrum assigned an isomer shift value of 0.00 mm/s. Samples run at room temperature and at 4.2 K had source and absorber at the same temperature. Samples run at Dry Ice–acetone and liquid nitrogen temperatures had the source at room temperature. No second-order Doppler correction was made in the data reported.